

CONTROLLING MELT POOL DIMENSIONS OVER A WIDE RANGE OF MATERIAL DEPOSITION RATES IN ELECTRON BEAM ADDITIVE MANUFACTURING

Emrecaan Soylemez and Jack L. Beuth

Department of Mechanical Engineering, Carnegie Mellon University
Pittsburgh, PA 15213

Karen Taminger

NASA Langley Research Center
Hampton, VA 23681

Abstract

Electron beam-based additive manufacturing processes are being seriously considered for manufacturing and repair applications in the aerospace industry. To be successful, these processes must work over a wide range of material deposition rates to combine affordability (requiring high deposition rates) with the ability to precisely deposit fine geometries (requiring low deposition rates). Melt pool size and shape are key characteristics to control in these processes. Control of melt pool dimensions will greatly increase the ability to successfully build shapes, and may play an important role in controlling solidification microstructure. In this paper, we present an analytically-guided approach for maintaining melt pool cross sectional area and thermal finite element simulation results are presented over a wide power range (1-5kW) to evaluate the approach. Single bead finite element simulations include the effects of temperature-dependent properties, latent heat, material addition and the distribution of power by a rapidly moving beam. Experiments were carried out on electron beam deposition equipment at NASA Langley Research Center and results show the same trends as those seen in the models. Ultimately, a map of curves of constant melt pool cross sectional areas and length-to-depth ratios is presented, covering power and velocity ranges over roughly a factor of 5.

Introduction

Laser and electron beam-based additive manufacturing processes are being seriously considered for manufacturing and repair applications in various industries. At the low power range, Laser Engineered Net Shaping (LENS[®]), which has been developed by Sandia National Laboratories and commercialized by Optomec[®], has been used to create complex prototypes, tooling, and small-lot production items with the ability to manufacture shapes based on geometry from CAD solid models [1]. Using a similar approach, Electron Beam Manufacturing (EBM) processes are being considered for manufacturing aerospace components. Like their laser-based counterparts, in EBM, parts or features are built up layer-by-layer with the beam serving as a moving heat source [2]. Electron beam-based processes offer added advantages over laser-based processes, including more efficient energy transfer to the substrate, transfer efficiencies that are not a function of the reflectivity of the substrate, the ability to deposit a wider range of materials, and the ability to rapidly move the electron beam across the surface or within the melt pool to locally tailor surface temperature fields.

An analytical solution related to these processes was derived by Rosenthal [3] and consists of a concentrated heat source moving across the surface of a semi-infinite half space. In this paper, Rosenthal models fitted to replicate results from finite element simulations are used to help interpret results and guide the selection of numerical simulations to perform. Previous work by the authors and their co-authors on beam-based SFF processes dates back more than a decade. Early work addressed the modeling and measurement of residual stress in metal and polymer deposition SFF processes [4-7]. Control of melt pool size under steady-state conditions for laser-based SFF processes has been considered by using a process map approach to plot melt pool size over the full range of process variables for LENS[®] [8-11]. The process map approach has been extended to consider melt pool size control under transient conditions and as a function of process size scale [12-15]. In the work on transient melt pool response, numerically determined melt pool response times are used to establish a lower bound on the response times of thermal feedback control systems. In the work on process size scale, the role of process size on the sensitivity of melt pool size to fluctuations in beam power or velocity are related to process robustness. The issue of residual stress control for laser-based SFF has also been addressed using a process map approach [16, 17]. In that work, a defined thermal gradient behind the melt pool is proposed as a means for predicting changes in final magnitudes of residual stress based on thermal simulation results. The work of [18] applies this approach to the concept of stress reduction by localized part preheating via a dual-beam laser or electron beam system.

Where this paper takes a broad process control approach to understanding EBM processes, other studies have focused on complex behavior inside the melt pool. A mathematical model of laser penetration during laser welding under keyholing conditions is presented in [19]. A 2-D axisymmetric incompressible, viscous transient model was coded to include the effects of surface tension and vaporization in [20]. Detailed mathematical models of melt pool behavior were derived in [21, 22] that include surface tension and natural convection inside the melt pool.

Material microstructure plays an important role in EBM process control, due to mechanical property requirements in finished parts. Rosenthal analytical calculations and finite element simulations have been used to observe cooling rates and thermal gradients, and their relation to grain morphology [23]. A study of process variable (beam power and velocity) effects shows that microstructure can vary significantly along the depth of the deposit, and that under high power conditions a transition from columnar to mixed or fully equiaxed structures is possible [24]. It was shown experimentally in [25] that melt pool size and cooling rate significantly depend on the travel velocity and laser power.

Sophisticated process models include the effect of material deposition on heat transfer conditions. In [26], 3-D simulations were performed using a dummy material method to model the addition of SS410 within the LENS power range. Following that, 2-D simulations were improved including wire feed effects [27]. This approach is similar to that used in the numerical modeling of this study, but the focus here is on mapping out melt pool dimensions over a broad power range (roughly 1-5kW) of interest in EBM.

Experiment-based optimization studies have been performed to optimize melt pool cross section size [28]. In this paper we consider the control of melt pool dimensions of cross sectional area and length via modeling that spans the full range of EBM power and travel speed

values of interest. Model predictions were followed by experiments for single bead deposition at NASA Langley Research Center.

Nomenclature

T	temperature
T_{base}	base plate temperature (and initial substrate temperature)
T_m	melting temperature
k	thermal conductivity
ρ	density
c	specific heat
L	melt pool length behind the maximum depth
Q or P	beam power
α	fraction of beam power absorbed by the substrate
V	beam travel speed
d	melt pool maximum depth
Area	melt pool maximum cross section area

Analytically-Based Approach To Find Constant Area For Single Bead Deposition

In this paper we will consider single bead deposition, presenting it as a building-block for the understanding of melt pool dimensional control in depositing complex geometries. In the EBM processes considered herein, material is added to the molten pool via a wire feed mechanism. Material deposition alters the geometry of the substrate and should be considered for its effect on melt pool size and shape. In general, melt pool sizes will be larger if the geometry of the deposited bead is included, due to a less direct conduction pathway into the substrate.

As will be shown in this paper, however, a Rosenthal-based analytical approach which neglects material addition, temperature dependent thermal properties and other physical effects of relevance in EBM processes can still be used as a guide to understand how changes in beam powers and velocities affect melt pool dimensions. Specifically, we use Rosenthal models with thermal properties chosen at a single temperature between T_{base} and T_m to allow the matching of a melt pool dimension with that predicted by a single sophisticated thermal finite element simulation. This “fitted Rosenthal” model is then used to predict the dependence of that melt pool dimension on beam power and velocity. Among other things, this allows the careful choosing of power and velocity combinations to model with the more cumbersome finite element models, which can take days to execute.

The goals of modeling single bead deposition are to identify baseline process variables for desired material deposition rates and bead geometries (as a quick reference guide for processing engineers), to identify process variable changes needed to maintain bead geometries as deposition rates are changed over wide ranges, and to greatly increase operating ranges. Achieving the final goal will allow consistent build conditions to be achieved under high material deposition rates for rapid, economical building of parts, and under low deposition rates for use in regions requiring geometric precision.

Figure 1 shows fitted Rosenthal analytical results for single bead deposition of Ti-6Al-4V. Each curve in the plot corresponds to beam power and velocity combinations yielding a constant melt pool cross sectional area. Values of melt pool cross sectional areas of 0.016, 0.031 and 0.063 in² are considered. Values for total melt rate, which is sum of molten material deposition rate and the rate of substrate melting, are provided in boxes for each of the 3 curves in 1kW intervals (from 2kW to 5kW). The curves of Fig. 1 were obtained by two fitted Rosenthal models over two power ranges. For beam powers at the substrate (αQ) larger than 3500W, Ti-64 thermal properties at 1523 K were used. For beam powers at or below 3500W, properties at 1200 K were used. Because of this, a slight discontinuity is seen in the shapes of the curves at a power of 3500W.

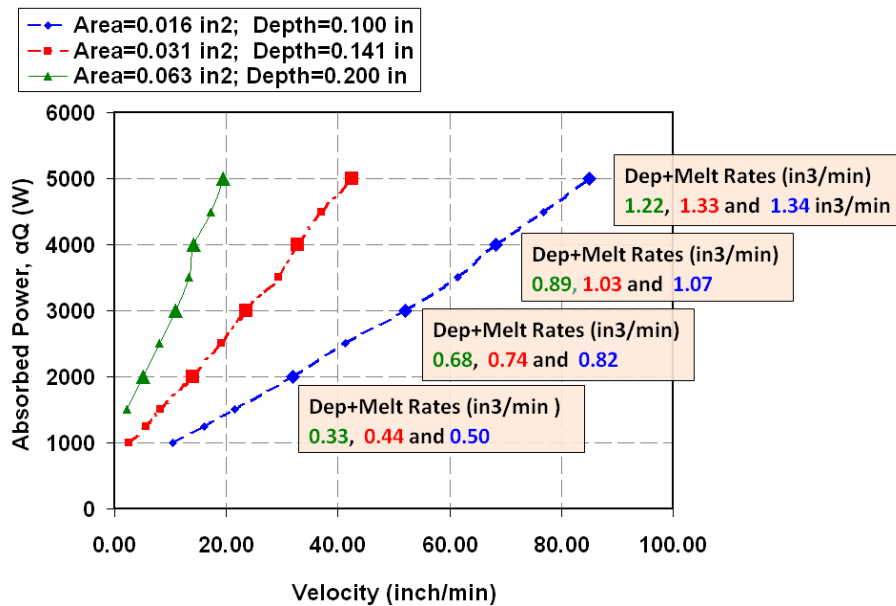


Figure 1. Analytical predictions for power and velocity combinations yielding constant cross sectional areas

The curves of Fig. 1 can be used by processing engineers by first specifying a material deposition rate in lb/hr or in³/min (9.5lb/hr is approx. 1 in³/min for Ti-64). For a given feed wire diameter, this fixes the wire feed rate. Next, a ratio of molten deposited material vs. substrate material must be specified. In work to date, a ratio of 1:0.30 has been used. This then determines the total rate of melting (for matching to values in the boxes). One finding of this work is that the total rate of melting is largely determined by the beam power. At each power level, the total melt rate values do not vary significantly between the green, red and blue curves (though the differences are greatest at 2kW). The final step in using the plot of Fig. 1 is to specify a melt pool (bead plus melted substrate) cross sectional area. This determines what curve to use, and determines the travel speed, V. Another way of thinking about the results of Fig. 1 is that the total rate of material melting is largely determined by the beam power. Beam velocity then determines whether you have a large melt pool moving slowly across the plate or a smaller melt pool moving rapidly across it, but in all cases the total rate of melting remains roughly the same.

The procedure outlined above allows use of the results of Fig. 1 to choose beam power, Q , and travel speed, V , for user-specified values of deposition rate, ratio of molten deposited material to substrate material, and melt pool cross sectional area. However, the plot is also a guide to maintaining melt pool area as beam power, beam velocity and material deposition rates are changed. To maintain bead cross sectional area while changing material deposition rate, beam power and velocity are increased or decreased while staying on a given curve. At the same time, wire feed rate is increased or decreased proportionally with beam velocity.

There are other ways that the results of Fig. 1 can be used. For instance, given a cross sectional image from a single bead deposition experiment with a length scale, it can be determined what processing curve deposition occurred on, based on bead and remelt cross sectional areas. Also, if a material deposition rate is given, travel velocity can be determined by dividing by the bead cross sectional area. Beam power can then be determined from the plot.

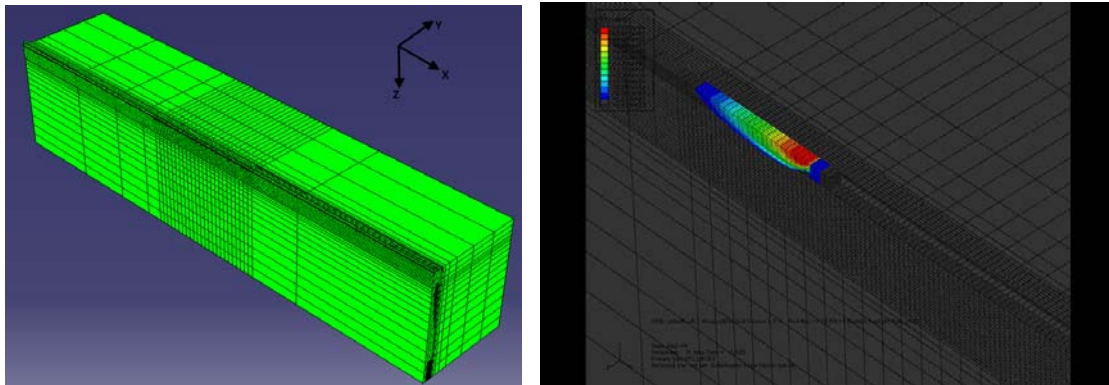
It is interesting to note that the curves of Fig. 1 are nearly straight lines. Thus, relatively simple rules of thumb can be formulated for use by processing engineers. The curves of Fig. 1 are not through the origin, however. This is due to a finite melt pool cross sectional area that exists as the velocity is reduced toward zero. A commonly used rule of thumb for e-beam or laser-based processes is that one can maintain deposition conditions over a range of powers and velocities by keeping the ratio of beam power to beam velocity constant. This is typically referred to as the “ $P/V = \text{constant}$ ” criterion. If this criterion were correct in predicting melt pool areas, the curves of Fig. 1 would be straight lines through the origin. The consequence of the results of Fig. 1 is that a $P/V = \text{constant}$ rule of thumb can give very poor results in small-scale processes (e.g. in the $< 1\text{kW}$ range) but it will become more accurate in understanding melt pool area control for large scale processes. In such cases, the offset of the curves from the origin has less of an effect.

Numerical Approach To Predict Constant Melt Pool Area For Single Bead Deposition

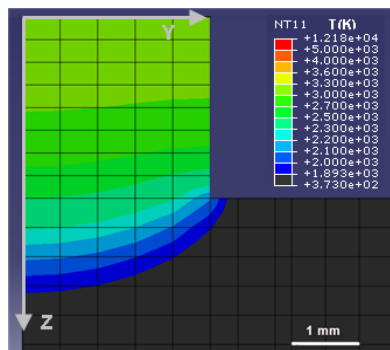
Three-dimensional finite element simulations have been performed to more precisely model single bead deposition, and to relate to the analytical results presented in Fig. 1. Two kinds of simulations were performed to obtain melt pool dimensions. The first type, designated as an added material simulation, uses the model change function in ABAQUS to directly simulate the addition of material by the wire feeder. In this type of simulation, all elements are defined and built initially, but elements in the added material portion of the model are deactivated using the remove function. After that, at each step, elements are added to simulate the addition of new bead material. In the current version of these models, the bead material existing during each load step extends 3 elements ahead of the heat source, which aids in the numerical solution and models heat transfer into some of the wire as it is fed into the melt pool. The second simulation type is designated as a constant bead model. In these models, the entire bead geometry is included in the simulation at all times. This greatly simplifies the modeling, and still captures many of the geometric features of the added bead. However, this allows heat transfer to occur well ahead of the melt pool in the bead material. Thus this type of model will tend to yield, for the same processing conditions, slightly smaller melt pool sizes than the more accurate added material simulations.

Consistent with deposition in a vacuum, these 3-D models do not include convective heat transfer on their vertical and top surfaces. The models have an initial temperature of 373 K and a constant temperature of 373 K specified at the base. Eight-noded linear brick elements are used throughout the model. A distributed heat flux along the top of the added bead is used instead of concentrated heat flux, more closely modeling oscillatory movement of the electron beam during deposition (which is used in experiments at NASA Langley to reduce the concentration of heat on the surface).

Figure 2(a) provides a far-field view of the 3-D mesh used for the symmetric added material and constant bead simulations. To reduce computational time, the mesh is biased toward the middle of the model, where steady-state melt pool sizes are determined. Figure 2(b) shows melt pool thermal contours from an added material simulation. Figure 2(c) illustrates the geometry of the added bead and melt pool maximum cross section shape, through a cross sectional view (in this case the heat source is moving out of the page).



(a) Added material and constant bead 3-D model geometry and mesh
 (b) Added material melt pool image



(c) Maximum cross section area of the melt pool (image is a cross sectional cut view of the geometry shown in (a) and (b))

Figure 2. Added material simulation images and temperature distribution near the melt pool

Numerical results for constant bead and added material models are given in Table 1 for comparison with Rosenthal analytical results used to generate the plot in Fig. 1. The melt pool cross sectional area values given in Table 1 show that, for high velocity cases (blue line), there

are no differences between constant bead and added material model results. For low velocity cases (green line) noticeable differences are seen. This is because, at high velocities, heat diffusion has no time to distribute heat ahead of the melt pool, so the additional material in the constant bead model does not affect the results. In comparing added material and Rosenthal analytical results, a similar trend is seen. High velocity (blue line) cases show very good correlation between the analytical and numerical models. Low velocity (green line) results show a significant difference, with the analytical results always being smaller than the corresponding numerical results. In these large cross sectional area cases, the geometry of the bead is having an effect on the results. The results of Table 1 thus indicate that the curves plotted in Fig. 1 are accurate representations of melt pool behavior, except for the green curve results, and particularly for the low power, low velocity cases on that curve.

Table 1. Comparisons between Rosenthal analytical results, constant bead model simulation results and added material simulation results

Melt Pool Cross Section Areas (in ²)		Fitted Rosenthal	Constant Bead Model	Added Material Model
Green Line	Case 1: $\alpha Q=5000W$; $V=19.4$ in/min	0.063	0.069	0.073
	Case 1: $\alpha Q=3000W$; $V=10.9$ in/min	0.063	0.068	0.079
	Case 1: $\alpha Q=2000W$; $V=5.2$ in/min	0.063	0.079	0.104
Red Line	Case 1: $\alpha Q=5000W$; $V=42.5$ in/min	0.031	0.033	0.032
	Case 1: $\alpha Q=3000W$; $V=23.6$ in/min	0.031	0.034	0.035
	Case 1: $\alpha Q=2000W$; $V=13.9$ in/min	0.031	0.034	0.037
Blue Line	Case 1: $\alpha Q=5000W$; $V=87.4$ in/min	0.016	0.016	0.016
	Case 1: $\alpha Q=3000W$; $V=52.0$ in/min	0.016	0.016	0.016
	Case 1: $\alpha Q=2000W$; $V=32.0$ in/min	0.016	0.017	0.017

Control Of Melt Pool Length To Depth Ratios

Melt pool cross sectional area is a key geometric quantity to control in EBM. It is related to bead cross sectional area and to melting depth into the substrate. Although the link between melt pool area and depth is not direct for cases of material addition (it depends on the bead geometry), for the Rosenthal model it is direct, with $A = \pi d^2/2$ (melt pool depth is simply the radius of the semicircular melt pool cross section). A second key geometric quantity is melt pool length, here defined as the length along the surface from the point corresponding to the maximum melt pool depth to the melt pool trailing edge. Experiments have shown that melt pool length can affect solidified deposited bead shape, consistent with its determining the geometry of the solidification front along the back of the melt pool. Along curves of constant melt pool area plotted in Fig. 1, melt pool lengths can change by a factor of more than 2. These facts have motivated a second study of melt pool length to depth or L/d ratios.

Table 2 presents added material numerical results for L/d ratios taken along the three constant melt pool cross sectional area curves of Fig. 1, with the curves corrected to agree with the more accurate added material finite element simulations. Using these results, a second order polynomial equation for L/d has been fitted along each of the 3 curves. These polynomial fits were then used to determine curves for constant L/d ratios, intersecting the curves for constant melt pool cross sectional areas. The final result of this work is presented in Fig. 3, which gives curves of not only constant melt pool areas, but also curves of constant L/d, all determined from added material finite element simulations.

Table 2. L/d ratios obtained from added material simulation results

	αQ (W)	Velocity (in/min)	L/d
Green Line	2000	10.1	3.16
	3000	14.1	4.63
	5000	23.2	6.27
Red Line	2000	17.1	3.38
	3000	25.8	5.13
	5000	44.5	8.80
Blue Line	2000	32.8	4.66
	3000	51.5	7.14
	5000	86.7	11.11

As shown in Fig. 3, curves of constant L/d are very much different than curves of constant melt pool cross sectional area, and, in fact, are nearly normal to the middle (red line) curve corresponding to a cross sectional area of 0.031 in². The plot of Fig. 3 now allows a processing engineer to not only identify beam powers and velocities to yield a desired melt pool cross sectional area, but to also then vary power and velocity to maintain that cross sectional area, or to maintain the current L/d ratio. Results shown in Fig. 3 demonstrate that for a specified material deposition rate (which roughly determines beam power) the high velocity (blue) curve yields the largest L/d values.

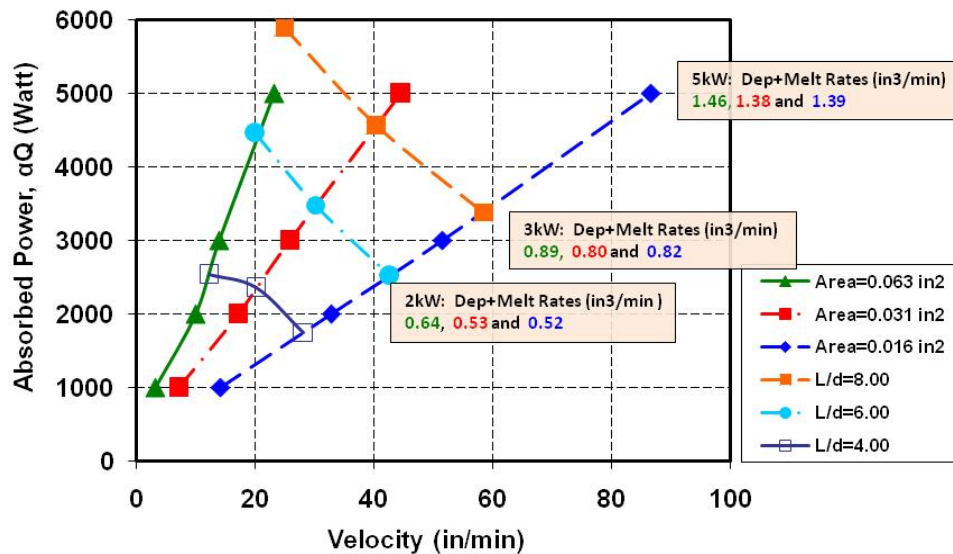


Figure 3. Lines of constant melted cross sectional areas and L/d ratios as determined by added material finite element simulations

Analogous predictions for L/d have been obtained using Rosenthal analytical calculations, yielding curves for constant L/d ratios. However, separate fitting of the results is needed for melt pool lengths and melt pool depths. To calculate melt pool length, Ti-64 properties at 992 K were used. For melt pool depth values, properties at 1523 K were used for cases with beam powers larger than 3500W. For beam powers at or below 3500W, properties at 1200 K were used (identical to that used for melt pool areas because the two dimensional quantities are linked for a Rosenthal model). Predictions were compared to those from added

material simulations plotted in Fig. 3. The comparison showed similar trends in results, but numerical values were not in good agreement. This was due to differences in melt pool lengths themselves, and due to differences in depth values for the same cross sectional areas (due to geometric differences). It was found that multiplying all Rosenthal-derived L/d values by a factor of 1.2 gave reasonable agreement with the added material simulation results in most cases, but not all. Overall, the use of fitted Rosenthal-based analytical formulas to predict melt pool cross sectional areas seems fairly robust. However, trying to use such a model to predict anything more than trends in melt pool lengths is not accurate.

Experimental Results

A collaboration between Carnegie Mellon and NASA Langley Research Center has allowed testing of the predictions provided in Fig. 1. Experiments were performed for single bead deposition using beam power and velocity combinations along each of the 3 curves presented in Fig. 1. Specimens were sectioned at two locations along the bead length in the steady-state portion of the bead. Figure 4 shows a typical cross sectioned bead image. Note that the boundary of the remelted portion of the substrate (designated by red arrows) is not the boundary of the entire discolored region of the substrate. That boundary designates the boundary of the heat affected zone.



Figure 4. Cross section micrograph showing the deposited bead, the remelted substrate boundary (see arrows) and the substrate heat affected zone

Experimental results for melt pool cross sectional areas are presented in Fig. 5. As the figure indicates, melt pool cross sectional areas were relatively constant. The exception to this finding is the lowest power case for the low velocity (green) line that is uppermost on the plot. Although this case is inconsistent with the Rosenthal-based curve for constant cross sectional area provided in Fig. 1, it is very much consistent with the more accurate finite element predictions presented in Table 1. This shows the value of including the geometric details of bead deposition in some cases. The agreement between the absolute numerical values for melt pool cross sectional areas and the experimental values is not very good, with experimental values always being higher (sometimes significantly so) than the predicted values. Investigations are underway to try to pinpoint the source of this disagreement. Regardless, however, the trends in the experiments clearly indicate the ability to control melt pool cross sectional areas over a very wide range of beam powers.

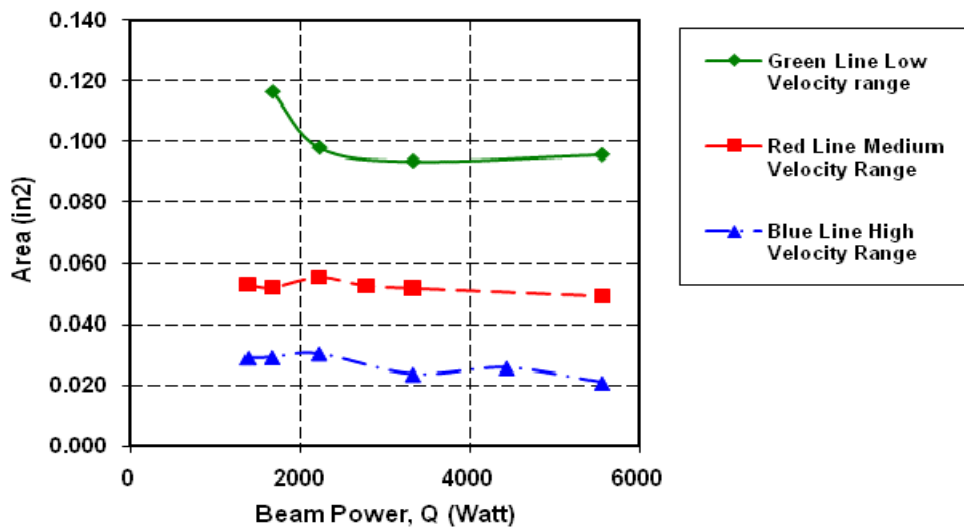


Figure 5. Experimental results presenting total (deposited+melted) cross section areas with changing power. Velocities were selected according to fitted Rosenthal calculations to obtain a constant area.

Conclusions

In this paper, analytical and numerical methods are used to map out combinations of beam powers and beam velocities for controlling melt pool dimensions in electron beam manufacturing (EBM) processes. The melt pool dimensions considered are melt pool cross sectional area and the ratio of melt pool length (L) to maximum depth (d). Results are presented which show specific paths through processing space to yield constant melt pool areas or L/d ratios. Experimental results are presented which show a clear ability to maintain melt pool cross sectional areas over a wide range of practical powers. Modeling results are also presented that demonstrate why a $P/V = \text{constant}$ rule of thumb for maintaining melt pool dimensions can yield poor results, particularly for small-scale processes.

Acknowledgements

The authors wish to acknowledge collaborations with Bryant and Raymond Walker of Keystone Synergistic Enterprises, Port St. Lucie, FL for additional experiments and physical insights related to this research. This research was supported by the National Science Foundation under grant CMMI-0700538, the Turkish National Ministry of Education and the Nick G. Vlahakis Graduate Fellowship.

References

1. Hofmeister, W., Griffith, M., Ensz, M., and Smugeresky, J., "Solidification in Direct Metal Deposition by LENS Processing," *JOM*, September 2001, pp. 30-35.
2. Taminger, K. M. B. and Hafley, R.A., "Characterization of 2219 Aluminum Produced by Electron Beam Freeform Fabrication," *Solid Freeform Fabrication Proceedings*, Proc. 2002 Solid Freeform Fabrication Symposium, Austin, August 2002, pp. 482-489.
3. Rosenthal, D., "The Theory of Moving Sources of Heat and Its Application to Metal Treatments," *Transactions of ASME*, Vol. 68, 1946, pp. 849-866.

4. Klingbeil, N.W., Zinn, J.W. and Beuth, J.L., "Measurement of Residual Stresses in Parts Created by Shape Deposition Manufacturing," *Solid Freeform Fabrication Proceedings*, Proc. 1997 Solid Freeform Fabrication Symposium, Austin, August 1997, pp. 125-132.
5. Klingbeil, N.W., Beuth, J.L., Chin, R.K, and Amon, C.H., "Measurement and Modeling of Residual Stress-Induced Warping in Direct Metal Deposition Processes," *Solid Freeform Fabrication Proceedings*, Proc. 1998 Solid Freeform Fabrication Symposium, Austin, August 1998, pp. 367-374.
6. Ong, R., Beuth, J.L. and Weiss, L.E., "Residual Stress Control Issues for Thermal Deposition of Polymers in SFF Processes," *Solid Freeform Fabrication Proceedings*, Proc. 2000 Solid Freeform Fabrication Symposium, Austin, August 2000, pp. 209-218.
7. Klingbeil, N.W., Beuth, J.L., Chin, R.K. and Amon, C.H., "Residual Stress-Induced Warping in Direct Metal Solid Freeform Fabrication," *International Journal of Mechanical Sciences*, Vol. 44, 2002, pp. 57-77.
8. Vasinonta, A., Beuth, J.L. and Griffith, M.L., "Process Maps for Laser Deposition of Thin-Walled Structures," *Solid Freeform Fabrication Proceedings*, Proc. 1999 Solid Freeform Fabrication Symposium, Austin, August 1999, pp. 383-391.
9. Vasinonta, A., Beuth, J.L., and Ong, R., "Melt Pool Size Control in Thin-Walled and Bulky Parts via Process Maps," *Solid Freeform Fabrication Proceedings*, Proc. 2001 Solid Freeform Fabrication Symposium, Austin, August 2001, pp. 432-440.
10. Vasinonta, A., Beuth, J.L. and Griffith, M.L., "A Process Map for Consistent Build Conditions in the Solid Freeform Fabrication of Thin-Walled Structures," *Journal of Manufacturing Science and Engineering*, Vol. 123, No. 4, 2001, pp. 615-622.
11. Beuth, J.L. and Klingbeil, N.W., "The Role of Process Variables in Laser-Based Direct Metal Solid Freeform Fabrication," *JOM*, September 2001, pp. 36-39.
12. Aggarangsi, P., Beuth, J.L., and Griffith, M.L., "Melt Pool Size and Stress Control for Laser-Based Deposition Near a Free Edge," *Solid Freeform Fabrication Proceedings*, Proc. 2003 Solid Freeform Fabrication Symposium, Austin, August 2003, pp. 196-207.
13. Birnbaum, A.J., Aggarangsi, P. and Beuth, J.L., "Process Scaling and Transient Melt Pool Size Control in Laser-Based Additive Manufacturing Processes," *Solid Freeform Fabrication Proceedings*, Proc. 2003 Solid Freeform Fabrication Symposium, Austin, August 2003, pp. 328-339.
14. Aggarangsi, P., Beuth, J.L., and Gill, D.D., "Transient Changes in Melt Pool Size in Laser Additive Manufacturing Processes," *Solid Freeform Fabrication Proceedings*, Proc. 2004 Solid Freeform Fabrication Symposium, Austin, August 2004, pp. 163-174.
15. Birnbaum, A.J., Beuth, J.L. and Sears, J.W., "Scaling Effects in Laser-Based Additive Manufacturing Processes," *Solid Freeform Fabrication Proceedings*, Proc. 2004 Solid Freeform Fabrication Symposium, Austin, August 2004, pp. 151-162.
16. Vasinonta, A., Beuth, J.L. and Griffith, M.L., "Process Maps for Controlling Residual Stress and Melt Pool Size in Laser-Based SFF Processes," *Solid Freeform Fabrication Proceedings*, Proc. 2000 Solid Freeform Fabrication Symposium, Austin, August 2000, pp. 200-208.
17. Vasinonta, A., Beuth, J.L., and Griffith, M.L. "Process Maps for Predicting Residual Stress and Melt Pool Size in the Laser-Based Fabrication of Thin-Walled Structures," *ASME Journal of Manufacturing Science and Engineering*, Vol. 129, No. 1, 2007, pp. 101-109.

18. Aggarangsi, P and Beuth, J.L., "Localized Preheating Approaches for Reducing Residual Stress in Additive Manufacturing," *Solid Freeform Fabrication Proceedings*, Proc. 2006 Solid Freeform Fabrication Symposium, Austin, August 2006, pp. 709-720.
19. Solana, P. and Ocana, J.L., "A Mathematical Model for Penetration Laser Welding as a Free-Boundary Problem," *Journal of Physics D: Applied Physics*, Vol. 30, No. 9, 1997, pp. 1300-1313.
20. Marathe, A.G, Ravi, M.R., "Simulation of Laser and Electron Beam Melting Problems." XVII National and VI ISHMT/ASME Heat and Mass Transfer Conference, 2004, pp. 57-62.
21. Simon, D. and Pal, U., "Mathematical Modeling of a Melt Pool Driven by an Electron Beam." *Metallurgical and Materials Transactions B*, Vol. 30, 2007, pp. 515-525.
22. Han, L., Liou, F.W., and Musti, S., "Thermal Behavior and Geometry Model of Melt Pool in Laser Material Process," *J. Heat Transfer*, Vol. 127, 2005, pp. 1005–1014.
23. Bontha, S., "The Effect of Process Variables on Microstructure in Laser-Deposited Materials," Ph.D. Thesis, Wright State University, June 2006.
24. Bontha, S., Klingbeil, N. W., Kobryn, P.A. and Fraser, H. L., "Effects of Process Variables and Size-Scale on Solidification Microstructure in Beam-Based Fabrication of Bulky 3D Structures," *Materials Science and Engineering A*, Vol. 513-514, 2009, pp. 311-318.
25. Wang, L., Felicelli, S. D., and Craig, J.E., "Experimental and Numerical Study of the LENS Rapid Fabrication Process," *Journal of Manufacturing Science and Engineering*, Vol. 131, No. 4, 2009, pp. 041019.1-041019.8.
26. Wang, L., Felicelli, S., Gooroochurn, Y., Wang, P. T. and Horstemeyer, M.F., "Optimization of the LENS process for Steady Molten Pool Size," *Materials Science and Engineering A*, Vol. 474, No. 1-2, 2008, pp. 148-156.
27. Yin, H., Wang, L., and Felicelli, S.D., "Comparison of Two-Dimensional and Three-Dimensional Thermal Models of the LENS Process," *Journal of Heat Transfer*, Vol. 130, No. 10, 2008, pp. 102101.1-102101.7.
28. Dey, V., Pratihar, D. K., Datta, G.L., Jha, M.N., Saha, T.K, and Bapat, A.V., "Optimization of Bead Geometry in Electron Beam Welding Using a Genetic Algorithm," *Journal of Materials Processing Technology*, Vol. 209, No. 3, 2009, pp. 1151-1157.